

# Magnetic turbulence in the plasma sheet

Z. Vörös (1), W. Baumjohann (1), R. Nakamura (1), M. Volwerk (1),  
 A. Runov (1), T. L. Zhang (1), H. U. Eichelberger (1),  
 R. Treumann (2), E. Georgescu (2), A. Balogh (3),  
 B. Klecker (2) and H. Rème (4)

(1) Institut für Weltraumforschung der ÖAW, Graz, Austria,

(2) Max-Planck-Institut für extraterrestrische Physik, Garching, Germany,

(3) Imperial College, London, UK,

(4) CESR/CNRS, Toulouse, France.

## Abstract

Small-scale magnetic turbulence observed by the Cluster spacecraft in the plasma sheet is investigated by means of a wavelet estimator suitable for detecting distinct scaling characteristics even in noisy measurements. The spectral estimators used for this purpose are affected by a frequency dependent bias. The variances of the wavelet coefficients, however, match the power-law shaped spectra, which makes the wavelet estimator essentially unbiased. These scaling characteristics of the magnetic field data appear to be essentially non-steady and intermittent. The scaling properties of bursty bulk flow (BBF) and non-BBF associated magnetic fluctuations are analysed with the aim of understanding processes of energy transfer between scales. Small-scale ( $\sim 0.08 - 0.3$  s) magnetic fluctuations having the same scaling index  $\alpha \sim 2.6$  as the large-scale ( $\sim 0.7 - 5$  s) magnetic fluctuations occur during BBF-associated periods. During non-BBF associated periods the energy transfer to small scales is absent, and the large-scale scaling index  $\alpha \sim 1.7$  is closer to Kraichnan or Iroshnikov-Kraichnan scalings. The anisotropy characteristics of magnetic fluctuations show both scale-dependent and scale-independent behavior. The former can be partly explained in terms of the Goldreich-Sridhar model of MHD turbulence, which leads to the picture of Alfvénic turbulence parallel and of eddy turbulence perpendicular to the mean magnetic field direction. Nonetheless, other physical mechanisms, such as transverse magnetic structures, velocity shears, or boundary effects can contribute to the anisotropy characteristics of plasma sheet turbulence. The scale-independent features are related to anisotropy characteristics which occur during a period of magnetic reconnection and fast tailward flow.

# 1 Introduction

Magnetic field measurements on board the Geotail and AMPTE/IRM spacecraft revealed that the power-law behaviour of the energy density spectra in frequency space,  $P(f) \sim f^{-\alpha}$  depends on the considered frequency range, both in the distant tail [Hoshino *et al.*, 1994], and in the near-Earth plasma sheet [Bauer *et al.*, 1995]. This finding was confirmed by Ohtani *et al.* [1995] using fractal analysis of the fluctuations in the AMPTE/CCE and SCATHA magnetic field measurements. The spectral index changes around  $f_{c1} \sim 0.01 - 0.08$  Hz. The observed scaling indices are  $\alpha_1 \sim 0.5 - 1.5$  for  $f < f_{c1}$  and  $\alpha_2 \sim 1.7 - 2.9$  when  $f > f_{c1}$  [Milovanov *et al.*, 2001; Volwerk *et al.*, 2003, 2004]. The uncertainty of the estimated values of  $\alpha_1$  and  $\alpha_2$  can be explained by slightly different frequency ranges studied by various authors and by the occurrence of spatially inhomogeneous, intermittent and transitory mechanisms involved in the generation of the observed scalings.

Since the characteristic timescale  $\sim 1/f_{c1}$  was found to be a few times the proton gyroperiod, ions can play an important role in the excitation of the corresponding magnetic fluctuations. The high-frequency part of the spectrum can be produced by an MHD cascading process. Instability mechanisms or self-organisation processes, such as coalescence of magnetic islands or inverse cascades were proposed for the explanation of low-frequency scaling [Hoshino *et al.*, 1994].

For frequencies higher than 0.1 Hz a second break in spectral power density was predicted theoretically at a turnover frequency  $f_{c2}$  [Milovanov *et al.*, 2001]. The estimation of the scaling index  $\alpha_3$  for frequencies  $f > f_{c2}$ , however, is encumbered by noise produced by the magnetometer itself. In this paper we examine those high frequency fluctuations for which the spectral indices  $\alpha_2$  and  $\alpha_3$  are expected. To this end we use a wavelet method which allows to estimate the scaling properties of magnetic fluctuations over the mentioned frequency ranges. Reliable spectral information could not be extracted, hitherto, from the noisy high-frequency magnetometer data. Nonetheless, in Section 2 we argue that an essentially unbiased wavelet method combined with an embedding technique of synthetic scaling signals allows us to estimate the scaling parameters reliably.

Very little is known about the origin of the multi-scale turbulence in the plasma sheet. Its appearance is obviously dependent on the driving and dissipation mechanisms which characterize an observed fluctuating process [Borovsky and Funsten, 2003]. Magnetic field and plasma flow fluctuations were observed by a number of authors [e.g., Coroniti *et al.*, 1980; Borovsky *et al.*, 1997; Neagu *et al.*, 2002]. Plasma shear flows might appear as possible drivers of those fluctuations. The statistical analyses of AMPTE/IRM data in the near-Earth magnetotail have already shown that there exist rapid plasma flows in the central plasma sheet which are preferentially perpendicular to the magnetic field and strongly sunward oriented

[Baumjohann *et al.*, 1989, 1990]. Subsequent research indicated that such flows are preferentially organized into sporadically occurring groups of bursty bulk flows (BBF), typically lasting for 10 min. Despite their short duration, BBFs are the carriers of decisive amounts of mass, momentum and magnetic flux [Angelopoulos *et al.*, 1992; Angelopoulos *et al.*, 1993; Schödel *et al.*, 2001]. Therefore BBFs can stir the plasma sheet plasma very efficiently. In this paper we place emphasis on comparison of multi-scale power and scaling properties of the magnetic fluctuations during BBF and non-flow or post-flow periods. We will also try to identify the turnover frequency  $f_{c2}$ , comparing the estimated values of  $\alpha_2$  and  $\alpha_3$  during BBF and non-BBF periods.

The observed scaling features, together with those expected from MHD considerations, will help us to classify the magnetic fluctuations observed by the Cluster spacecraft in the plasma sheet. Recent approaches to MHD turbulence highlight the influence of a mean magnetic field on scale-dependent appearance of anisotropic fluctuations [Goldreich and Shridhar, 1995]. The anisotropy increases towards small scales. Therefore, the high-resolution Cluster magnetometry provides a way for studying the scale-dependent anisotropy of magnetic fluctuations. We discuss the observed magnetic anisotropies in terms of recent MHD theories and simulations.

## 2 The wavelet estimator

We analyse the scaling properties of 67 Hz resolution magnetic field fluctuations from the Cluster fluxgate magnetometer [Balogh *et al.*, 2001] using a wavelet method proposed by Abry *et al.*, [2000]. Wavelets offer an effective way for getting an unbiased estimate of  $\alpha$  [Veitch and Abry, 1999], whereas power spectral estimations are affected by frequency-dependent multiplicative bias [Abry *et al.*, 1995]. The spectral estimation is biased mainly because it is performed over a constant bandwidth which does not match the  $f^{-\alpha}$  structure of the spectrum properly. The variance of discrete wavelet coefficients (see later), however, matches well the power-law shaped spectrum. Unlike Fourier methods, wavelet methods work better for processes exhibiting spectral scaling because wavelets have inbuilt rescaling properties. The wavelet estimator allows to identify different kinds of scaling processes which are invisible to biased spectral estimators, especially in noisy and short data.

## 2.1 Outline of the method

Abry *et al.*, [2000] proposed a semi-parametric wavelet technique based on a fast pyramidal filter bank algorithm for the estimation of scaling parameters  $c_f$  and  $\alpha$  in the relation  $P(f) \sim c_f f^{-\alpha}$ , where  $c_f$  is a nonzero constant. The algorithm consists of several steps. First, a discrete wavelet transform of the data is performed over a dyadic grid  $(scale, time) = (2^j, 2^j t)$  and  $j, t \in \mathbf{N}$ . Then, at each octave  $j = \log_2 2^j$ , the variance  $\mu_j$  of the discrete wavelet coefficients  $d_x(j, t)$  is computed through

$$\mu_j = \frac{1}{n_j} \sum_{t=1}^{n_j} d_x^2(j, t) = 2^{j\alpha} c_f C(\alpha, \psi_0) \quad (1)$$

where  $n_j$  is the number of coefficients at octave  $j$ , and  $C(\alpha, \psi_0) = \int f^{-\alpha} |\psi_0(f)|^2 df$ ,  $\psi_0(f)$  stands for the power spectrum of the mother wavelet  $\Psi_0$ . Finally, from Equation (1)  $\alpha$  and  $c_f$  are estimated by constructing a plot of  $y_j \equiv \log_2 \mu_j$  versus  $j$  (logscale diagram, LD) and by using a weighted linear regression over the region  $(j_{min}, j_{max})$  where  $y_j$  is a straight line. In this paper we use the Daubechies wavelets for which finite data size effects are minimized and the number of vanishing moments  $M$  can be changed. The latter allows to cancel or decrease the effects of linear or polynomial trends and ensures that the wavelet details are well defined.

We note that the wavelet estimator, Equation (1), is also affected by a multiplicative bias (multiplication by  $C(\alpha, \psi_0)$ , see later), but  $C$  is not frequency dependent. A similar multiplicative term for spectral estimators is frequency dependent, which makes the log-log plot of the power versus frequency not precisely linear. Therefore the estimation of  $\alpha$  via linear regression in the log-log plot is strongly affected by bias [Abry *et al.*, 1995]. Within the wavelet approach Veitch and Abry [1999] have found explicit solutions for the variances of  $\log_2(\mu_j)$  which are then used in the weighted regression in the LD. These improvements make the wavelet estimator unbiased even for data of small length.

Different kinds of scaling can be analysed by this technique. The value of  $\alpha$  and the scaling range  $(j_m, j_n)$  are characteristic for the specific scalings present [Abry *et al.*, 2000]. For example  $\alpha \in (0, 1)$  at the largest scales present in the data is characteristic for long range dependent processes, while  $\alpha \sim 0$  at large scales together with  $\alpha \in (0, 1)$  at small scales is a signature of noise. Furthermore,  $\alpha \in (1, 3)$  aligned at almost all scales available corresponds to a nonstationary, self-similar (fractal) process having a fractal dimension  $D = (5 - \alpha)/2$  [Abry *et al.*, 2000].

## 2.2 An embedding technique

When the scaling index is estimated over a high frequency range, magnetometer noise can strongly influence the outcome. Since different estimation techniques used over slightly different frequency ranges, there is a large scatter in the previously observed values of  $\alpha$ , which makes it difficult to compare the scaling properties in turbulence. Furthermore, the estimated values are presumably affected by the occurrence of transitory processes in the plasma sheet. We therefore perform the estimation of  $c_f$  and  $\alpha$  within sliding overlapping windows of width  $W$  with a time shift  $S \ll W$  to analyse the data over different frequency ranges with the same method and simultaneously take into account their temporal evolution.

In order to examine how the signal-to-noise ratio (SNR, the relative power of the signal and the noise in LD) influences the estimation of  $\alpha$  within the window  $W$  in small-scale fluctuations, we generate a self-similar fractal signal with known second order scaling properties using wavelets and embed it in a time series of quiet time magnetic field measurements from the Cluster spacecraft. As a synthetic fractal signal we use fractional Brownian motion (fBm) generated by a fast filter bank based pyramidal algorithm [Abry and Sellan, 1996]. Fractional Brownian motion has a Gaussian distribution of increments by definition. At the same time, magnetic fluctuations exhibit two-point Gaussian statistics only for large separations. Therefore, we consider the fBm process as an approximation which can roughly model the second order properties of the magnetic fluctuations.

We suppose that the magnetic fluctuations observed in the plasma sheet during quiet times are close to the magnetometer noise level. Figure 1a shows the magnetic field  $B_X$  component (67 Hz resolution) observed by Cluster 3 on September 7, 2001. If not specified the GSM coordinate system will be used throughout the paper. Two short fractal signals  $A$  and  $B$ , with the same scaling index  $\alpha_A \equiv \alpha_B = 1.6$  but different amplitude are added to  $B_X$ . In Figure 1a  $B_X$  is depicted from 1840 to 1917 UT. First, signal  $A$  is added into  $B_X$  from  $\sim 1857$  to  $\sim 1901$  UT. The average amplitude of fluctuations of  $A$  is much larger than of  $B_X$ . In Figure 1b a dashed horizontal line shows the theoretical value of  $\alpha_A \equiv \alpha_B = 1.6$ . The estimated  $\alpha_A$  reaches this theoretical value in a wider interval in Figure 1b as was the length of signal  $A$  in Figure 1a. Despite the non-precise timing, the estimated value of  $\alpha_A$  is correct. Next, signal  $B$  is embedded into  $B_X$ . Signal  $B$  and  $B_X$  have comparable average amplitude. The estimated  $\alpha_B$  in Figure 1b does not achieve the theoretical horizontal line, therefore  $\alpha_B$  is underestimated. We can conclude that, whenever the amplitude of the signal is significantly larger than the amplitude of the noise (case A), the correct value of  $\alpha$  is recovered, otherwise  $\alpha$  is underestimated (case B).

Let us explain now the reason of non-precise timing. In Figure 1b  $\alpha_s$  are esti-

mated within a sliding window  $W \sim 480$  s over time scales (octaves)  $j_1 = 2$  and  $j_2 = 4$  ( $\sim 0.08 - 0.33$  s and  $\sim 3 - 12$  Hz; these are approximate Fourier periods and frequencies that correspond to the main oscillations within the Daubechies wavelets). The embedded fractal signals A and B produce a rapid departure of the estimated values  $\alpha$  from the noise level  $\alpha \sim 0.3$ , as soon as the analysing window includes some part of a fractal signal (A or B in Figure 1a). This effect is visible at  $\sim 1853$  UT and before 1906 UT, when two analysing windows depicted by horizontal lines in Figure 1b are centered in those time positions. The dashed, vertically extended right and left ends of the windows match perfectly the beginnings and the ends of the fractal signals A and B. When the timing is important, the effect of window length has to be accounted.

Another effect which influences the estimation of the scaling index  $\alpha$ . If the duration of a scaling process  $T$  is less than half the window length,  $W/2$ ,  $\alpha$  is also underestimated. In Figure 1a the length of the fractal signals A and B equals  $W/2$ . The proper sliding window length for unbiased estimation of  $\alpha$  can be found by trial. For decreasing  $W$  the estimated  $\alpha$  increases, then saturates. Obviously, as  $W$  decreases, the fluctuations of the estimations increase. In general,  $W$  has to be chosen such that the opposing requirements for robustness of scaling parameter estimations (wide window needed) and for time localization of short events (narrow window needed) were matched. For the events analysed in this paper  $W = 61$  s was found to be an optimal choice.

Finally, let us consider possible kinds of non-physical mechanisms which can lead to spurious scalings. Time series analysis methods may lead to spurious results when applied to short data series containing irregularities, e.g. jumps, spikes [Katsev and L'Heureux, 2003] or random pulse trains [Watkins *et al.*, 2001]. Spikes, i.e., single values with large deviation are removed during quality check of the data. Possible effects of other irregularities will be discussed jointly with the estimation of the scaling parameters in subsequent sections.

### 2.3 Noise correction

The above explained embedding technique allows us to introduce corrections, whenever the amplitude of a fractal signal approaches the noise level. It can happen when high frequency (small-scale) scalings are examined. A few more steps are needed to explain the method in detail. To this end we show the typical scaling properties of a fractal signal ( $s$ ), noise ( $n$ ) and of a compound additive process (signal+noise,  $sn$ ) in LD. For what follows the subscripts  $s, n, sn$  will correspond to the specified processes. We also demonstrate that a single correction curve (see later) belongs to every embedded model fractal signal with a given  $\alpha_s$ .

Equation 1 describes the scaling properties of a signal through the scaling of

the corresponding wavelet coefficients. Taking a base 2 logarithm of both sides of Equation 1, we obtain an equation of line in LD. Therefore any scaling signal (a straight line in LD) can be characterized by a pair of values  $(c_f(j), \alpha(j_{min}, j_{max}))$ , where  $c_f(j)$  is the power of intercept at octave  $j$ . Here we suppose that, for a fixed mother wavelet, the last term,  $C(\alpha, \psi_0)$ , on the right hand side of Equation 1, is dynamically unimportant. The change of  $\psi_0$ , however, can influence the estimation of scaling parameters. We use the Daubechies family of wavelets with changing number of vanishing moments  $M$ . It does slightly influence our estimations and the corresponding uncertainties represent a source of error.

Figure 2 shows an exemple of LD. The magnetometer noise is depicted by a single curve, since we suppose, it is time-independent (see later). It exhibits signatures typical for noise:  $\alpha_n \sim 0$  at large scales ( $j > 7$ ) together with  $\alpha_n \sim 0.3 \in (0, 1)$  at small scales ( $j < 6$ ) [Abry *et al.* 2000]. For the sake of clarity the straight lines corresponding to the scalings of both signal and compound process are depicted only at the left hand side of Figure 2 ( $j \leq 5$ ). The amplitude of the model fractal signal was changed from values larger to values smaller than the amplitude of the noise. The resulting parallel, shifted straight lines are representations of self-similar signals in LD. The compound process exhibits similar characteristics as the signal itself, while SNR is large. If SNR becomes  $\leq 1$ , the compound process approaches the straight line of noise at the scales  $j_1$  and  $j_2$ .

Time-independent noise has averages  $(\langle c_{fn}(j) \rangle, \langle \alpha_n(j_1, j_2) \rangle) \sim const.$  Our goal is to estimate the time evolution of the scaling exponent of the signal  $\alpha_s(j_1, j_2, t)$  for known  $(c_{fn}, \alpha_n)$  and  $(c'_{fsn}(j, t), \alpha_{sn}(j_1, j_2, t))$ . The normalization  $c'_{fsn}(j, t) \equiv c_{fsn}(j, t) / \langle c_{fn}(j) \rangle$  ensures that for weak signals,  $c_{fsn} \sim c_{fn}$  (noise dominates), and  $c'_{fsn} \sim 1$ . Actually,  $c'_{fsn}(t)$  represents a time dependent SNR.

Now we can use the introduced notation and the embedding technique to study the dependence of  $\alpha_{sn}$  on  $c'_{fsn}$  within a window  $W$ . Figure 3 shows the relationship  $\alpha_{sn}(c'_{fsn})$  (correction curves), which was obtained experimentally by embedding two model fractal signals with  $\alpha_{mod} = 1.5$  and 2, gradually decreasing their amplitudes (decreasing SNR), into quiet time  $B_X$  measured by s/c 4 on September 7, 2001. For both model fractals the correction curves were computed at the octaves  $j = 0$  and  $j = 4$ , separately. Independent of  $j$ ,  $\alpha_{sn}$  approaches asymptotically  $\alpha_s \equiv \alpha_{mod}$  for large enough  $c'_{fsn}$ . Large  $c'_{fsn}$  means that SNR is large and the compound signal exhibits the same scaling as the fractal model signal (left-top straight lines in Figure 2). If  $c'_{fsn} \sim 1$ , the noise dominates, and  $\alpha_{sn} \sim \alpha_n$  (scaling of the compound process between  $y_j = -5$  and  $-10$  in Figure 2). Between the two limits ( $c'_{fsn} \rightarrow \infty$  and  $c'_{fsn} \sim 1$ ), however, the course of the curves for  $j = 0$  and  $j = 4$  in Figure 3 is rather different. Because of the complex behaviour of the compound process at  $j = 0$  near the noise level (Figure 2),  $\alpha_{sn}$  cannot be deter-

mined from the  $\alpha_{sn}(c'_{fsn})$  relationship unequivocally (Figure 3). Since the relation is unambiguous at the scale  $j = 4$ , we will consider the  $\alpha_{sn}(c'_{fsn})$  curves at that octave throughout the paper.

The accuracy of the wavelet method estimation of  $\alpha$  can be controlled by the power of intercept of the compound process  $c'_{fsn}$ . Figure 3 shows that for  $c'_{fsn} \ll 100$  we find  $\alpha_{sn} < \alpha_{mod}$ , therefore  $\alpha_s$  is underestimated. The  $\alpha_{sn}(c'_{fsn})$  relationship allows us to introduce corrections and estimate the effective asymptotic value of  $\alpha_s$ .

We note that  $c_{fsn}(t)$  and  $\alpha_{sn}(j_1, j_2, t)$  are computed directly from magnetic field time series by using a sliding window  $W$ . The key assumption of the method is time-independence of the scaling parameters for noise. Obviously, this condition is not strictly fulfilled. Therefore, it is important to examine the time-independence of  $\langle c_{fn} \rangle$  and  $\langle \alpha_n \rangle$ . The parameters  $c'_{fsn}(t)$  and  $\alpha_{sn}(j_1, j_2, t)$  computed from magnetic field  $B_X$  component (67 Hz resolution) observed by the Cluster spacecraft s/c 1 and 3 during the quiet interval 1700-2100 UT on September 7, 2001, are depicted in Figure 4. Here  $W = 68$  s and  $S = 4$  s. During the chosen interval the spacecraft are traversing the neutral sheet from the northern ( $B_X \sim 18$  nT) to the southern hemisphere ( $B_X \sim -15$  nT) (Figure 4a) and the plasma flow velocity does not exceed 50 km/s (not shown). Independent of the location of the Cluster spacecraft and despite the occurrence of low frequency wave motion after 1830 UT, both  $\alpha_{sn}(j_1, j_2, t)$  and  $c'_{fsn}(t)$  exhibit stationary behaviour, fluctuating around the mean values (Figure 4 b,c). The estimated  $\alpha_{sn}$  can be related to the magnetometer noise  $\alpha_n$  because  $\alpha_{sn} \sim \alpha_n \in (0, 1)$  and  $c'_{fsn} \sim c_{fn} \sim 1$  (see also Figure 3). Noteworthy is that  $\alpha_n$  and  $c_{fn}$  are slightly different for each s/c (Figure 4b,c) and also vary with the magnetic field components. The examination of several quiet time magnetic field time series and time series obtained from ground-based calibration measurements shows that in average (including the four s/c and each magnetic component)  $\langle \alpha_n \rangle = 0.5 \pm 0.25$  and  $\langle c_{fn} \rangle = 0.004 \pm 0.003$ . Similar values were obtained using 128 Hz quiet time magnetic field measurements from the Equator-S spacecraft (not shown). For discrimination between  $\alpha_s$  (which is expected to be  $> 1$ ) and  $\alpha_n$ , this accuracy seems to be sufficient. It is expedient in concrete case studies, however, to compute the correction curves (Figure 3) for each spacecraft and component separately.

Examining  $\alpha_{sn}$  and  $c'_{fsn}$  estimated for  $B_X$  from s/c 2 on September 7, 2001, we found short, but significant deviations from  $\langle \alpha_n \rangle$  and  $\langle c_{fn} \rangle$ , respectively (not shown). The deviations occurred due to a 5 min long data gap on s/c 2, which led to spurious scalings because of the step function-like irregularity in  $B_X$ , in accordance with the findings of *Katsev and L'Heureux* [2003]. This type of spurious estimations can easily be avoided by interpolation. Another type of jump-related



spurious estimation might occur near the plasma sheet boundary layer (PSBL) or owing to its motion. The PSBL cannot be identified from the magnetic field measurements alone [Eastman *et al.*, 1984]. Therefore, non-physical scalings due to magnetic jumps near PSBL are not expected.

In summary, using the wavelet approach, we can estimate directly from a time series the time evolution of the parameters of a compound process  $(c'_{fsn}(t), \alpha_{sn}(t))$ . The time independent parameters of noise  $(\langle c_{fn} \rangle, \langle \alpha_n \rangle)$  can be obtained from quiet time measurements. When  $c'_{fsn}(t)$  is small, the effective asymptotic value of  $\alpha_s(t)$  for a self-similar signal can be obtained from a correction curve taking a limit  $c'_{fsn}(t) \rightarrow \infty$ . Spurious estimations during quiescent periods can be avoided by careful quality checks of the magnetic data.

### 3 Magnetic fluctuations in the plasma sheet

In order to introduce the wavelet method and the small-scale corrections to the estimated  $\alpha$ , quiet time magnetic measurements together with artificial fractal signals were used in the previous section. Since our goal is to investigate BBF and non-BBF related magnetic turbulence, here we choose a  $\sim 4$ h interval during which the Cluster spacecraft observed BBF and non-BBF intervals successively.

#### 3.1 Event overview and small-scale corrections

In what follows, we analyse burst mode (67 Hz) magnetic data from the Cluster fluxgate magnetometer (FGM) [Balogh *et al.*, 2001] during the interval 0110-0500 UT on August 27, 2001, when the Cluster spacecraft were near the  $Z_{GSM} = 0$  plane, in the postmidnight magnetotail ( $X_{GSM} \sim -19R_E$ ). The magnetic data are compared with the spin-resolution (4 s) velocity data from the Cluster ion spectrometry (CIS/CODIF) experiment [Réme *et al.*, 2001]. Figure 5a shows the  $B_X$  component from s/c 1,3. The variation of the scaling index for two different ranges of scales is depicted in Figure 5b. In addition to  $(j_1, j_2) = (2, 4)$ , corresponding time scale  $\sim 0.08 - 0.33$  s, we also consider the octaves:  $(j_3, j_4) = (5, 8)$ , corresponding time scale  $\sim 0.7 - 5$  s. Hereinafter we will refer to those scales as small scales  $(j_1, j_2)$  and large scales  $(j_3, j_4)$ , respectively. Obviously,  $j_1$  is limited by the resolution and  $j_4$  by the chosen window  $W$ . The average noise levels  $\langle \alpha_n \rangle$  for s/c 1,3 and  $B_X$  magnetic components are also indicated by black and gray dashed lines in Figure 5b. The large-scale scaling exponents are anticorrelated with the magnitude of  $B_X$  simply because of the preferential occurrence of perpendicular flows closer to the neutral sheet ( $B_X \rightarrow 0$  nT). Figure 5c shows the variation of the normalized power of the intercepts  $c'_{fsn}$  computed for the small scales  $(j_1, j_2)$ .

Its time evolution exhibits periods of  $c'_{fsn} \sim 1$  intermittently interrupted by bursts of activity when  $c'_{fsn} > 1$ . The former corresponds to the noise level, indicating that there is no significant energy flow from large scales into small scales. The increased values of  $c'_{fsn}$  are associated with high frequency (small-scale) fluctuations of  $B_X$  (Figure 5a), increased  $\alpha_{sn}$  (relative to  $\langle \alpha_n \rangle$ , Figure 5b) and are well correlated with the appearance of bursty perpendicular flows (Figure 5d). The large scales ( $j_3, j_4$ ) are not corrupted significantly by magnetometer noise.

The effect of spurious estimations due to spikes, random pulses, or other types of nonstationary signals can be addressed for BBF-associated periods, too. The use of Daubechies analysing wavelets with vanishing moments ensures that part of the nonstationarities represented by polynomial trends are cancelled. Spurious estimates of the scaling index might appear because of discontinuities which separate earthward moving plasma structures from the background plasma ahead of them [Sergeev *et al.*, 1996]. In fact, before the appearance of the rapid perpendicular flow, e.g., at 0131 UT (Figure 5d), there is a large jump in the large scale scaling index from  $\alpha_{sn}(j_3, j_4) \sim 1$  to 2.5. This jump and all similar jumps in our data can partly be explained by the presence of a discontinuity in front of the plasma flow [Nakamura *et al.*, 2002]. On the other side, this short effect cannot be separated from the non-physical effect of the sliding window, explained above (Figure 1).

After 0130 UT,  $\alpha_{sn}(j_3, j_4)$  fluctuates around  $\sim 2.5$  for more than 30 min (Figure 5b). We believe, that all estimations exhibiting small fluctuations around a mean value for equal or longer time than the sliding window length ( $\sim 1$  min), belong to a BBF-associated scaling process in our case. Therefore these estimations are not spurious. The same is true for non-BBF associated processes. Also,  $\alpha_{sn}$  is largely coherent between s/c1 and 3. Short living pulses are supposed to be random, however. Moreover, some results of multifractal approach [Vörös *et al.*, 2003] and of wavelet based structure function approach [Vörös *et al.*, 2004] also support the idea that BBF-associated magnetic fluctuations correspond to a physical scaling process.

During the BBF-associated periods one finds that  $1 < c'_{fsn} < 100$ , therefore  $\alpha_s$  is underestimated (see Figure 3). Since self-similarity is defined for  $1 < \alpha < 3$ , we used 4 model fractal time series with  $\alpha_{mod} = 1.5, 2, 2.5, 3$  and quiet time  $B_X$  magnetic data from s/c 1,3 to compute the  $\alpha_{sn}(c'_{fsn})$  correction curves at the octave  $j=4$  (Figure 6). These curves can be used to introduce corrections and to estimate the effective value of  $\alpha_s$ . Like in Figure 3 there are two limiting cases. The condition  $c'_{fsn} \rightarrow \infty$  leads to  $\alpha_{sn} = \alpha_s = \alpha_{mod}$ , with slower approach to a model value for  $\alpha_{sn} > 2$ . The limit  $c'_{fsn} \rightarrow 1$  leads to  $\alpha_{sn} = \langle \alpha_n \rangle$ . The error bars depicted at the left-top corner of Figure 6 arise from the uncertainty of the estimation of  $\alpha_{sn}$  in a logscale diagram using Daubechies wavelets with

varying number of vanishing moments ( $M = 3 - 7$ ) and from the uncertainty of the magnetometer noise level estimation within the chosen window  $W$ . The depicted error bars represent only the uncertainty of the determination of the correction curves, and not the uncertainty of the estimations of  $\alpha_s(j_1, j_2)$ . The estimation error of the small scale  $\alpha$  changes from  $\pm 0.2$  to  $\pm 0.5$  as  $c'_{fsn} \rightarrow 1$ . The errors can be estimated by adding more correction curves to Figure 6 (not shown). It is more difficult to distinguish an  $\alpha$  as  $c'_{fsn}$  decreases. We present two examples how to read the measured  $\alpha_{sn}(j_1, j_2)$  using both Figures 5 and 6. The two dashed lines A and B in Figure 6 correspond to two pairs of values  $(c'_{fsn}, \alpha_{sn})$  in Figure 5b,c before 0330 UT. The gray lines and the letter A belong to s/c 3, while the black lines and the letter B belong to s/c 1. In both examples the corrected effective value of small-scale  $\alpha_s(j_1, j_2)$  is close to the correction curves which asymptotically reach the horizontal line  $\alpha_{mod} = 3$  in Figure 6. After correction, all BBF associated peaks of  $\alpha_s(j_1, j_2) > \langle \alpha_n \rangle$  and  $c'_{fsn} > 1$  show a similar feature (not shown), that is in average,  $\alpha_s(j_1, j_2) = 2.5 \pm 0.5 \sim \alpha_s(j_3, j_4) \sim 2.5$ . Therefore, after introducing corrections, the BBF-associated small-scale and large-scale scaling indices cannot be discriminated. We note that the peaks at  $\sim 0240$  UT from s/c 1 (Figure 5b,c) appear due to the data gaps.

### 3.2 Statistical evaluation of BBF and non-BBF associated multi-scale magnetic fluctuations

During non-BBF periods  $\alpha_s(j_3, j_4)$  drops to the noise level when s/c 1,3 are in the lobe ( $B_X \sim 25$ nT) or fluctuates between 1 and 2.5 when s/c 1,3 are in the plasma sheet (Figure 5a,b). Among others, the time evolution of the scaling indices can be influenced by the location of the Cluster spacecraft, the duration and the magnitude of perpendicular flows and by the motion of the plasma sheet (e.g., thickening or thinning). Despite the complexity, we can separate BBF and non-BBF associated magnetic fluctuations, based on two different conditions.

Condition 1 is based only on small-scale scaling parameters having for BBF-associated fluctuations on both s/c 1,3,  $\alpha_{sn}(j_1, j_2) > \langle \alpha_n \rangle + 0.3$  and  $c'_{fsn} > 2$  and non-BBF-associated fluctuations  $\alpha_{sn}(j_1, j_2) < \langle \alpha_n \rangle + 0.1$  and  $c'_{fsn} < 1.1$ . It simply means that we relate the observed small-scale magnetic fluctuation-dissipation activity to the large-scale magnetic fluctuations. We suppose that on the basis of scaling characteristics and power of small-scale magnetic fluctuations we can identify BBF and non-BBF associated intervals without actual examination of velocity data. For testing this supposition we use only the parameters computed from the magnetic field  $B_X$  component measured by s/c 1,3 (Figure 5a-c). So we select only those values of  $\alpha_s(j_3, j_4)$  from the whole period (Figure 5b) which meet the above conditions for  $\alpha_{sn}(j_1, j_2)$  and  $c'_{fsn}$ . The conditional statistics performed on

the large-scale scaling index gives for both s/c 1,3  $\alpha_{s,BBF}(j_3, j_4) = 2.57 \pm 0.05$  for BBF-associated and  $\alpha_{s,non-BBF}(j_3, j_4) = 1.6 \pm 0.4$  for non-BBF associated case.

Now we consider also the velocity data. Condition 2 is based on thresholding of perpendicular flows, taking  $V_{\perp,xy} \equiv \sqrt{V_{\perp,x}^2 + V_{\perp,y}^2} > 300$  km/s for rapid flows and  $V_{\perp,xy} < 100$  km/s for non-BBF associated remnant flows. Since the velocity data is available with a time resolution of  $\sim 4$  s and the time step between neighbouring sliding windows is  $S = 4$  s, after adjusting times,  $\alpha_s(j_3, j_4)$  can be compared to  $V_{\perp,xy}$ . It gives  $\alpha_{s,BBF}(j_3, j_4) = 2.6 \pm 0.1$  and  $\alpha_{s,non-BBF}(j_3, j_4) = 1.7 \pm 0.4$ . All the estimates represent mean values with standard deviations.

Both conditions give the same statistical results on large-scale scaling index. From the conditions and the corresponding values of large-scale indices follows that, relative to non-BBF associated intervals, BBF-associated intervals exhibit both large-scale and small-scale spectral steepening and an unambiguous increase of small-scale power of magnetic fluctuations. Therefore we propose that small-scale magnetic fluctuations are energized by BBF's. Then the spectral transfer of energy to small scales is transient, which makes the position of the spectral break at the expected turnover frequency  $f_{c2}$  uncertain. Our results suggest that whenever BBF-associated magnetic fluctuations occur, the break at  $\sim f_{c2}$  disappears when the small-scale corrections are introduced. Otherwise the energy flow to small scales ends at  $f_{c2}$ , and in this case, at frequencies  $f > f_{c2}$ , the measured scaling parameters belong to the noise. The examination of the LD's at various ranges of scales shows that  $f_{c2}$  may correspond to the approximate Fourier frequencies of 1 – 3 Hz (between octaves  $j_2$  and  $j_3$ ).

The same analysis of the  $B_Y$  and  $B_Z$  magnetic field components shows that the observed scaling features remain similar to the  $B_X$  case. The small-scale  $B_Y$  and  $B_Z$  fluctuations are also associated mainly with  $V_{\perp,xy}$ . After introducing corrections as above,  $\alpha_s(j_1, j_2) \sim \alpha_s(j_3, j_4) \sim 2.6$  for BBF and  $\sim 1.7$  for remnant flows, the errors in the same range as above, in conditional statistics of  $B_X$ . A dissimilarity appears in  $B_Z$  small-scale fluctuations (Figure 7). The small-scale power  $c'_{fsn}$  of  $B_Z$  fluctuations (Figure 7c) during BBF-associated intervals is several times larger than that of  $B_X$  (Figure 5c) or  $B_Y$  (not shown). Usually  $c'_{fsn}(B_Z) \gg c'_{fsn}(B_Y) > c'_{fsn}(B_X)$  over time scales less than 1 s. This is a signature of anisotropy and we will examine it deeper.

### 3.3 Anisotropy of magnetic fluctuations

The small-scale powers of the magnetic field components from s/c 1,3, computed at  $j = 4$  ( $\sim 0.33$  s), are compared in log-log scatterplots in Figure 8. The comparison of  $B_X$  and  $B_Y$  components shows a balanced scatter around the line

$c'_{fsn}(B_X) = c'_{fsn}(B_Y)$  (Figure 8a), though the increased population of points under that line between  $2 < c'_{fsn}(B_Y) < 10$ , indicates a weak anisotropy. The scatterplot of  $c'_{fsn}(B_X)$  and  $c'_{fsn}(B_Z)$  shows strong anisotropy (Figure 8b) for values  $c'_{fsn} > 1.5$ . We also calculated the scatterplots at scale  $j = 6$  ( $\sim 1.3$  s) (Figures 9 a, b), which, after comparison with Figure 8b, indicate scale dependent anisotropy. The anisotropy increases towards small scales. Since  $c'_{fsn}(B_Z) \gg c'_{fsn}(B_X)$  and  $c'_{fsn}(B_Y) \geq c'_{fsn}(B_X)$  in Figure 8, the small-scale magnetic fluctuations are generated due to multi-scale transfer of energy preferentially in the GSM  $Z$  or  $Z - Y$  direction. The powers at the scale  $j = 6$  show more isotropy, even if the scatterplot of  $c'_{fsn}(B_X)$  versus  $c'_{fsn}(B_Y)$  (Figure 9a) indicates that, with increasing scales the field-aligned power of fluctuations can also increase.

The points depicted by '+' signs in Figures 8b and 9b belong to the time period between 0400 and 0410 UT. During this interval a magnetic reconnection event in the central plasma sheet at 0401 UT was identified by *Baker et al.* [2002]. The corresponding '+' points in Figures 8b and 9b, therefore, are associated with the magnetic reconnection or/and the tailward flow, leading to a strong anisotropy which does not exhibit the same increase towards the small scales as it is observed for the other points. Therefore the underlying mechanism which drives these fluctuations should be different from the previous scale dependent one. Since only this reconnection-related short interval shows different anisotropy characteristics, we cannot say more about the nature of the underlying physical processes. Answering the question about reconnection or tailward flow associated anisotropy characteristics certainly requires a thorough statistical analysis. We can speculate, however, that the observed scale-independent anisotropy features might be related to the specific current systems or magnetic field topology near the reconnection site [*Nagai et al.*, 2003; *Runov et al.*, 2003].

The small-scale  $\alpha_{sn}(j_1, j_2)$  for individual components are compared in scatterplots in Figure 10 a,b. Again,  $\alpha_{sn}(j_1, j_2, B_Z)$  seems to be different from  $\alpha_{sn}(j_1, j_2, B_X)$  and  $\alpha_{sn}(j_1, j_2, B_Y)$ . This anisotropy can weaken, however, because non-corrected values are depicted and the corrections are larger for  $B_X, B_Y$  than for  $B_Z$  (Figures 5c and 7c).

The anisotropy can also be considered in the coordinate system of the local mean field. We computed the mean total magnetic field vector through low-pass filtering the GSM magnetic field components and using standard vector operations transformed the burst mode magnetic data into mean-field perpendicular ( $B_{\perp}$ ) and mean-field aligned ( $B_{\parallel}$ ) components. Figures 11a, b show  $B_{\perp}$  and  $B_{\parallel}$ , respectively, computed for averaged  $\langle B \rangle$  at the time-scale 1.3 s. Figures 11 c, d show the perpendicular  $c'_{fsn}(B_{\perp})$  and the parallel  $c'_{fsn}(B_{\parallel})$  powers, computed at the scales  $j = 3$  ( $\sim 0.33$  s) and  $j = 6$  ( $\sim 1.3$  s). As above for the GSM  $X, Y, Z$  components

(Figures 8-10), the anisotropy is scale dependent and the small-scale power preferentially develops in directions perpendicular to the mean magnetic field. Again, the short interval after 0400 UT shows a different kind of reconnection or tailward flow related behavior. The large-scale ( $j = 6$ ) perpendicular power remains larger than the parallel power only during this interval. The similarity of the statistical results obtained in GSM and mean field coordinate systems can be explained as follows: for open, stretched magnetic field lines  $B_{\parallel}$  resembles  $B_X$  and  $B_{\perp}$  is similar to  $\sqrt{B_Z^2 + B_Y^2}$  (where  $B_Y$  and  $B_Z$  are the GSM components of the magnetic field). Dissimilarities can appear close to the neutral sheet when  $B_X \rightarrow 0$ .

### 3.4 Two-point conditional statistics

Let us investigate now the effect of the transitory character of the fluctuations or their drivers. We compare magnetic fluctuations observed at the same time on two spatially separated Cluster spacecraft. Figure 12 compares the parallel  $\alpha_{s\parallel}(j_3, j_4)$  and the perpendicular  $\alpha_{s\perp}(j_3, j_4)$  scaling indices from s/c 1 and 3. The scatterplot in (Figure 12a) involves all the magnetic data from s/c 1,3 and forms an irregular cloud of points. We applied two-point conditional statistics to find BBF- and non-BBF-associated points in that cloud. We used the same small-scale condition 1 combined with the velocity condition 2 as above (both should give the same results), and required the fulfilment jointly at s/c 1,3 at the same time. In consequence of the joint conditional requirement the amount of data points in (Figures 12 b,c) is significantly reduced. It can be explained partially by a relatively high level of fluctuations of the considered parameters. For example, the perpendicular velocity wildly fluctuates during the rapid flows (e.g. Figure 5d) which makes the comparison with the small-scale parameters more difficult. The omission of the velocity condition, however, does not add many more points to the Figures 12 b,c. Therefore, we suppose that fewer joint data points are found by two-point conditional statistics because the two spacecraft are often in physically different regions, exhibiting different scaling features. It indicates that the magnetic fluctuations and their sources are transient and limited in space.

The statistical evaluation of the BBF-associated data points in Figure 12b gives averages  $\alpha_{s\perp}(j_3, j_4) = 2.4 \pm 0.3$  and  $\alpha_{s\parallel}(j_3, j_4) = 2.7 \pm 0.3$  which is consistent with the previous estimations using the components  $B_{X,Y,Z}$  (dashed lines). The '+' signs in Figure 12b represent measurements during the reconnection event, discussed above.

Figure 12c shows the non-BBF-associated data points. Here the '+' signs represent measurements near the plasma sheet boundary layer or in the lobe ( $B_X \geq 20$  nT) while the remaining points are inside of the plasma sheet ( $B_X \leq 15$  nT). The statistical evaluation of the latter gives  $\alpha_{s\perp}(j_3, j_4) = 1.7 \pm 0.3$  and  $\alpha_{s\parallel}(j_3, j_4) =$

$1.7 \pm 0.4$ , which is again consistent with the previous estimations using the components  $B_{X,Y,Z}$  (dashed lines).

Let us summarize the main results at the end of this section. We used a wavelet method to study the small-scale properties of magnetic fluctuations. We found that the energy transfer to the smallest available time scales is associated with BBFs. The scaling properties of those fluctuations are recoverable from burst mode magnetic fluctuations by using an embedding technique. Small-scale fluctuations show an increased anisotropy relative to the mean magnetic field. The anisotropy is observed mainly in the normalized power of the magnetic fluctuations, while it is less evident in the spectral scaling index. The transient character of the physical processes or driving mechanisms makes a robust estimation of the basic characteristics of magnetic turbulence difficult in the plasma sheet.

## 4 Discussion

A complete characterization of MHD turbulence requires not only a statistical description of the velocity field, but also a statistical study of other measurable quantities, e.g. magnetic field, density or temperature fluctuations. In this paper we analysed a 4 hour long period of high quality burst mode (67 Hz) magnetic field data, which allowed an immersion to the scale or frequency ranges which are not available in velocity measurements. We considered time scales from  $\sim 0.08$  to 5 s, which, assuming 500 km/s velocities during rapid flows, correspond roughly to spatial scales of 40 – 2500 km in the flow direction. The average velocities are smaller than 500 km/s, so the largest scale can be significantly smaller than 2500 km. Also, both the velocities and the estimated spatial scales are smaller in other than the maximum velocity direction or during non-BBF intervals. Since the average separation of the Cluster spacecraft was  $\sim 1500$  km during 2001, we used principally a single-point technique to analyse scaling characteristics of magnetic fluctuations from s/c 1,3. The usual multi-point statistical approach, commonly available in laboratory measurements, is not available in the plasma sheet at those scales and the conversion of the scaling characteristics of magnetic fluctuations in time into scaling laws in wavenumber space is possible only through additional hypotheses. The Taylor hypothesis assumes that the conversion is possible if the spatial fluctuations on a given scale pass over the spacecraft faster than they typically evolve in time. In the plasma sheet this can be the case during fast BBF's [Horbury, 2000] or during strong global bulk flows which may occur after a dynamical reconfiguration of the magnetotail [Borovsky and Funsten, 2003]. Otherwise, the random velocities of the fluctuations advect spatial structures over the spacecraft. A more realistic approach is the so-called random sweeping model (RSM), which

takes the basically random velocities of the flow into account and allows to obtain statistical information on spatial structures.

*Borovsky et al.* [1997] have used RSM and found that the spectral index, describing the scaling properties of magnetic fluctuations in the plasma sheet at the frequency range of  $1/4 - 1/150 \text{ s}^{-1}$ , is the same in both frequency or wavenumber representations, that is,  $k^{-\alpha} \sim f^{-\alpha}$ . The 'large-scale' ( $\sim 1/0.3 - 1/5 \text{ s}^{-1}$ ) used in this paper partially overlaps with the scales of *Borovsky et al.* [1997] paper. Note that, RSM is supposed to work when the large scale velocity field drives the small-scale fluctuations. This seems to be valid in our case due to the high correlation between BBFs and small-scale magnetic fluctuations. Therefore we suppose, that at least at the scales  $(j_3, j_4)$  the equality  $k^{-\alpha} \sim f^{-\alpha}$  holds also in our case and the estimated values of  $\alpha$  can be compared with the power-law dependence of power spectra in MHD turbulence. We have to underline, however, that RSM is only a model and its validity should be proven comparing real spatial and time structures. In absence of such comparisons the interpretation of scaling indices in terms of MHD turbulence remains disputable. At the same time, we consider the observed anisotropy effects to be more reliable. Let us start the comparison of observations and theory, therefore, with the evaluation of the influence of a local mean magnetic field on anisotropy of fluctuations.

The clear signs of the interaction of rapid flows with the magnetic field in the plasma sheet are the BBF-associated dipolarization of field lines (increase of  $B_Z$ ) and the breaking and diversion of the flows around the dipolar inner magnetosphere. The presence of a mean magnetic field in the plasma sheet cannot be eliminated by coordinate transformations. This is in contrast with hydrodynamic turbulence, where the anisotropy usually ceases in the coordinate system of the average flow [*Biskamp*, 2003]. The classical Kolmogorov theory for hydrodynamic and the Iroshnikov-Kraichnan theory for MHD turbulence assume isotropy of the inertial-range energy cascade in Fourier space, exhibiting scalings  $E(k) \sim k^{-5/3}$  and  $\sim k^{-3/2}$ , respectively ( $E(k)$  is the amount of energy between wavenumbers  $k$  and  $k + dk$  divided by  $dk$ ).

*Shebalin et al.* [1983] studied incompressible MHD anisotropies arising in wave vector space in the presence of a mean magnetic field. They studied the interaction of opposite-travelling wave packets and found that, in wave vector space, those interactions produce modes with wavevectors preferentially perpendicular to the mean magnetic field. *Goldreich and Sridhar* [1995] proposed a balance condition between parallel and perpendicular modes (parallel propagating Alfvén waves and perpendicular eddy motions). On this basis it was shown that a scale dependent anisotropy appears, namely  $k_{\parallel} \sim k_{\perp}^{2/3}$  (or  $l_{\parallel} \sim l_{\perp}^{2/3}$ , where  $l \sim 1/k$  is the characteristic scale of eddies in parallel and perpendicular directions), which means



that the anisotropy is increasing with decreasing scale. Moreover, it was shown that the perpendicular fluctuations exhibit Kolmogorov scaling  $E(k) \sim k^{-5/3}$ . In other words, the mean magnetic field does not influence the perpendicular hydrodynamic cascade formed by eddies. The coupled parallel fluctuations are essentially produced by waves. In the case of compressible MHD the Alfvén modes follow the anisotropic Goldreich-Sridhar scaling while fast modes exhibit isotropy [Cho *et al.*, 2003].

The scale dependent anisotropy proposed by Goldreich and Sridhar [1995] would represent a way the relative importance of Alfvén waves and eddy motions might be recognized. Matthaeus *et al.* [1998] tested this assumption using Fourier spectral methods for MHD equations in a periodic cube. They have found, that for incompressible, weakly compressible and driven MHD turbulence, anisotropy scales linearly with the ratio of fluctuating to total magnetic field strength. Their results therefore seem to be inconsistent with the Goldreich-Sridhar model. Cho and Vishniac [2000] argued, however, that the Fourier technique used by Matthaeus *et al.* [1998] smooths out the true scaling relation for anisotropy. It happens because the anisotropic eddies or wave packets are elongated along magnetic field lines. When they follow the large-scale variation of the magnetic field, they point in different directions. Consequently, the information about the eddy shapes is lost when a global transformation such as the Fourier transformation is applied. Cho and Vishniac [2000] showed that, when the eddy shapes relative to the local magnetic field are analysed in real space, the Goldreich-Sridhar scaling is recovered.

For what follows, it is important that not only the velocity statistics exhibits the Goldreich-Sridhar anisotropy, but also the magnetic field statistics [Cho and Lazarian, 2004]. If we suppose similarity between frequency and wavenumber scalings, then our results suggest that the observed magnetic turbulence in the plasma sheet also resembles the anisotropy of Goldreich-Sridhar model. The small-scale magnetic turbulence is stronger in perpendicular directions. It is mainly visible when the relative powers of fluctuations are compared (Figures 8 and 11). Then, except for the short interval when magnetic reconnection and tailward flow occurs, the anisotropy is scale dependent (Figures 8,9). The applied wavelet technique ensures that the scale-dependent anisotropy is not smoothed out. Namely, over each considered scale range the local trend (local mean field) is cancelled by the analysing wavelet having a proper number of vanishing moments. The observed anisotropy seems to indicate that the small-scale eddy turbulence is stronger than the Alfvénic turbulence. This is in agreement with the results of Borovsky and Funsten [2003], who claimed that turbulence of eddies rather than the turbulence of Alfvén waves prevails in the plasma sheet. Their observation is based on three different arguments: (a.) Alfvén wave turbulence produces scale sizes that are larger than the vertical size of the plasma sheet, whereas eddy turbulence does not;

(b.) the autocorrelation length of the turbulence is typical for eddy turbulence; (c.) the low Alfvén ratio (ratio of the kinetic energy of the flow to the energy density of magnetic fluctuations) indicates 2D eddy structures. All these results might yield a picture of the Goldreich-Sridhar model and quasi-2D MHD turbulence. The quasi-2D MHD picture is supported by numerical studies of high Reynolds number turbulence which predict that the spatial distribution of the turbulent fields is more intermittent in 2D than in 3D MHD ([Biskamp, 2003], and references therein). Since BBF-associated magnetic fluctuations are stretched down to the small scales  $(j_1, j_2)$  (Figures 5,7), where the anisotropy becomes stronger and turbulence might be essentially 2D, an increase of the small scale intermittence can be expected, too. Indeed, Vörös *et al.* [2003] have shown that small scale magnetic field intermittence increases during BBF-associated intervals. Here, some more words of caution have to be added. First of all, the importance of multi-scale dynamics in turbulence has to be underlined. Since the Goldreich-Sridhar anisotropy is scale dependent, at sufficiently large scales this kind of anisotropy can disappear, and even Alfvénic turbulence can become stronger. Figures 9a and 11 d show that the large scale power of parallel ( $B_X$  or  $B_{\parallel}$ ) fluctuations can be equal with or slightly overpower the perpendicular components ( $B_Y, B_Z$  or  $B_{\perp}$ ). The development of anisotropy and 2D structures can also be dependent on the actual Reynolds numbers, helicity, Alfvén ratio [Oughton *et al.*, 1994] or be influenced by the presence of transverse pressure-balanced magnetic structures or transverse velocity shears [Ghosh *et al.*, 1998]. In this respect it is important to note that in our case the mean field direction is constantly changing due to the time-varying contribution of magnetic field components to the total magnetic field (compare Figures 5,7). Nevertheless, the small scale power of the  $B_Z$  (vertical) fluctuations is the strongest all the time. The vertical GSM direction, however, is not always the perpendicular direction to the mean magnetic field. Therefore the effect of the mean field, even if it represents a robust way for the development of scale-dependent anisotropy has to be complemented by other mechanisms, which can produce strong fluctuations in perpendicular directions. For example the above mentioned transverse magnetic structures or velocity shears can also redirect the initially parallel-propagating Alfvén waves to highly oblique waves [Ghosh *et al.*, 1998]. In the plasma sheet, BBF-associated dipolarization, increase of  $B_Z$  (or  $B_Y$  when the current sheet is tilted), can represent such a transverse magnetic structure. Also, the relative thinness of the plasma sheet in the  $z$  direction and the associated boundary effects can produce anisotropy statistics in plasma sheet turbulence [Vörös *et al.*, 2004]. To evaluate the possible contributions of these mechanisms a wider statistical study is required, however.

Let us consider now the estimated scaling indices  $\alpha$  in comparison with the predictions of Goldreich-Sridhar model. When the anisotropy effects are neglected,

the conditional statistics explained above gives for BBF-associated flows the large scale index  $\alpha_s(j_3, j_4) = 2.6 \pm 0.1$ , independent on magnetic field component. It is definitely different from the Goldreich-Sridhar model which predicts Kolmogorov scaling with  $\alpha \sim 5/3$  in perpendicular direction. We could advance an argument that the Goldreich-Sridhar anisotropy is weaker at the scales  $(j_3, j_4)$ , but the small-scale  $\alpha_s(j_1, j_2)$  reaches the same range of values when the estimated  $c'_{fsn}$  is large enough and allows to introduce corrections.  $\alpha_s(j_3, j_4)$  decreases and approaches the Kolmogorov scaling during non-flow or post-BBF intervals, when the ratio of the large-scale mean field to the magnetic fluctuations becomes larger and the conditions for the development of Goldreich-Sridhar anisotropy are more favourable. In this case the estimated  $\alpha_s(j_3, j_4) = 1.7 \pm 0.4$ . The large error appears because the post-flow intervals usually correspond to transient, probably decaying turbulence. This also causes that one cannot distinguish between the Kolmogorov and Iroshnikov-Kraichnan models. The high value of  $\alpha_s(j_3, j_4)$  during BBF-associated intervals does not necessarily mean that the Goldreich-Sridhar phenomenology fails. Magnetic fluctuations are subject to an additional constraint which acts during rapid flows only. The limited vertical dimension of the flow channel or the plasma sheet thickness can modify the actual value of  $\alpha$  increasing it to  $\alpha \sim 3$ , which is a limiting value for fully developed 2D hydrodynamic turbulence [Volwerk *et al.*, 2003, 2004, Vörös *et al.*, 2004].

## 5 Conclusions

The work described here demonstrates the ability of the windowed wavelet estimator for obtaining reliable estimates of the effective second-order scaling parameters  $(c_f, \alpha)$  even in situations when the noise level is relatively high. Magnetic turbulence seems to be steady only during relatively short time intervals (a few minutes), otherwise  $\alpha$  exhibits nonstationary behaviour at all scales, which can partially explain the large scatter of previously estimated values of scaling indices. As we observed magnetic turbulence associated with bursty flows and post-flow intervals, our findings agree well with previous knowledge that the flow of plasma in the Earth's magnetotail is intrinsically unsteady [*e.g.* Baumjohann, 2002]. Joint conditional statistics from two Cluster spacecraft s/c 1,3 shows a high level of spatial intermittence which is related to the differing scaling features in physically different regions in the plasma sheet.

The examination of BBF-associated high frequency magnetic fluctuations within a sliding window showed that the small-scale  $(j_1, j_2)$  and large-scale  $(j_3, j_4)$  scaling indices are equal within error estimations. Volwerk *et al.* [2003, 2004] have obtained similar scaling exponents for the time scales 1-13 s. It means that the

spectral break predicted by *Milovanov et al.* [2001] for the scales  $< 1/f_{c2} \sim 10$  s is absent and, using the notation from the Introduction,  $\alpha_2 \sim \alpha_3$ . During non-BBF periods the small-scale  $\alpha_3 \sim \alpha(j_1, j_2)$  approaches the noise level of the magnetometer, which introduces an artificial break at the scale  $\sim 1$  s. Obviously, it cannot be interpreted in terms of a new scaling regime describing a scale dependent physics.

We found that, for the scales analysed, the conversion of the observed scalings from frequency to wavenumber representation is model dependent and cannot be verified by direct comparison of spatial and temporal variations. It makes the interpretation of the results in terms of MHD phenomenology more difficult. The anisotropy features of magnetic fluctuations provided additional tools to facilitate the interpretation of the results. The anisotropy is better visible in the normalized power of fluctuations  $c_f$  than in the scaling index  $\alpha$ . It was shown that large-scale magnetic fluctuations are more isotropic while small-scale magnetic turbulence evolves in direction perpendicular to the mean magnetic field, usually in the GSM  $Z$  or  $Z - Y$  direction, and the observed anisotropy is scale dependent. It partly agrees with the predictions of Goldreich-Sridhar model of MHD turbulence, but the additional effect of transverse magnetic structures or velocity shears cannot be excluded. On this basis we think the turbulence in the plasma sheet is a mixture of Alfvénic wavy turbulence and of eddy 2D turbulence. The latter becomes stronger and more intermittent with decreasing scales.

The occurrence of reconnection and/or rapid tailward flow can increase the level of anisotropy. The build-up of a flow channel seems to modify the actual value of the scaling indices, indicating the presence of additional constraints on Alfvénic and/or eddy turbulence. These are observations which should be verified on larger data sets.

#### *Acknowledgement*

The authors acknowledge the use of the code for the estimation of scaling exponents developed by P. Abry and his colleagues.

## References

- [1] Abry, P., P. Gonçalves, and P. Flandrin, Wavelets, spectrum estimation and 1/f processes, *Wavelets and Statistics*, edited by A. Antoniadis, and G. Oppenheim, *Lect. Notes Stat.*, 103, 15, 1995.
- [2] Abry, P., and F. Sellan, Some remarks on and fast implementation for the wavelet-based synthesis of fractional Brownian motion proposed by F. Sellan and Y. Meyer, *Appl. Comput. Harmon. An.*, 3, 377, 1996.

- [3] Abry, P., P. Flandrin, M.S. Taqqu, and D. Veitch, Wavelets for the analysis, estimation and synthesis of scaling data, *Self-Similar Network Traffic and Performance Evaluation*, edited by K. Park, and W. Willinger, Wiley Interscience, New York, 39, 2000.
- [4] Angelopoulos, V., W. Baumjohann, C. F. Kennel, F. V. Coroniti, M. G. Kivelson, R. Pellat, R. J. Walker, H. Lühr, and G. Paschmann, Bursty bulk flows in the inner plasma sheet, *J. Geophys. Res.*, *97*, 4027, 1992.
- [5] Angelopoulos, V., et al., Characteristics of ion flow in the quiet state of the inner plasma sheet, *Geophys. Res. Lett.*, *20*, 1711, 1993.
- [6] Baker, D.N., et al., Timing of magnetic reconnection during a global magnetospheric substorm onset, *Geophys. Res. Lett.*, *29*(24), 2190, doi:10.1029/2002GL015539, 2002.
- [7] Balogh, A. et al., The Cluster magnetic field investigation: overview of in-flight performance and initial results, *Ann. Geophys.*, *19*, 1207, 2001.
- [8] Bauer, T. M., W. Baumjohann, R. A. Treumann, N. Sckopke, and H. Lühr, Low-frequency waves in the near-Earth plasma sheet, *J. Geophys. Res.*, *100*, 9605, 1995.
- [9] Baumjohann, W., G. Paschmann, and C. A. Cattell, Average plasma properties in the central plasma sheet, *J. Geophys. Res.*, *94*, 6597, 1989.
- [10] Baumjohann, W., G. Paschmann, and H. Lühr, Characteristics of high-speed ion flow in the plasma sheet *J. Geophys. Res.*, *95*, 3801, 1990.
- [11] Baumjohann, W., Modes of convection in the magnetotail, *Phys. Plasmas*, *9*, 3665, 2002.
- [12] Biskamp, D., Magnetohydrodynamic turbulence, Cambridge Univ. Press, 2003.
- [13] Borovsky, J. E., R. C. Elphic, H. O. Funsten, and M. F. Thomsen, The Earth's plasma sheet as a laboratory for flow turbulence in high- $\beta$  MHD, *J. Plasma Phys.*, *57*, 1, 1997.
- [14] Borovsky, J. E., and H. O. Funsten, MHD turbulence in the Earth's plasma sheet: Dynamics, dissipation and driving, *J. Geophys. Res.*, *108*, 1284, doi:10.1029/2002JA009625, 2003.
- [15] Cho, J., and E. T. Vishniac, The anisotropy of magnetohydrodynamic Alfvénic turbulence, *Astrophys. J.*, *539*, 273, 2000.

- [16] Cho, J., and A. Lazarian, Compressible magnetohydrodynamic turbulence: mode coupling, scaling relations, anisotropy, viscosity-damped regime, and astrophysical implications, *Mon. Not. R. Astron. Soc.*, in press, 2004.
- [17] Cho, J., A. Lazarian, and E. T. Vishniac, MHD turbulence: scaling laws and astrophysical implications, *Lect. Notes Phys.*, 614, 56, 2003.
- [18] Coroniti, F. V., L. A. Frank, D. J. Williams, R. P. Lepping, F. L. Scarf, S. M. Krimigis, and G. Gloeckler, Variability of plasma sheet dynamics, *J. Geophys. Res.*, 85, 2957, 1980.
- [19] Eastman, T. E., L. A. Frank, W. K. Peterson, and W. Lennartsson, The plasma sheet boundary layer, *J. Geophys. Res.*, 89, 1553, 1984.
- [20] Goldreich, P., and S. Sridhar, Toward a theory of interstellar turbulence. II. Strong Alfvénic turbulence, *Astrophys. J.*, 438, 763, 1995.
- [21] Ghosh, S., W. H. Matthaeus, D. A. Roberts and M. L. Goldstein, The evolution of slab fluctuations in the presence of pressure-balanced magnetic structures and velocity shears, *J. Geophys. Res.*, 103, 23691, 1998.
- [22] Hoshino, M., A. Nishida, T. Yamamoto, and S. Kokubun, Turbulent magnetic field in the distant magnetotail: Bottom-up process of plasmoid formation? *Geophys. Res. Lett.*, 21, 2935, 1994.
- [23] Horbury, T. S., Cluster II analysis of turbulence using correlation functions, *ESA SP-449*, 89, 2000.
- [24] Katsev, S., and I. L’Heureux, Are Hurst exponents estimated from short or irregular time series meaningful?, *Comput. Geosci.*, 29, 1085, 2003.
- [25] Matthaeus, W. H., S. Oughton, S. Ghosh, and M. Hossain, Scaling of anisotropy in hydromagnetic turbulence, *Phys. Rev. Lett.*, 81, 2056, 1998.
- [26] Milovanov, A. V., L. M. Zelenyi, G. Zimbardo, and P. Veltri, Self-organized branching of magnetotail current systems near the percolation threshold, *J. Geophys. Res.*, 106, 6291, 2001.
- [27] Nakamura, R., et al., Motion of the dipolarization front during a flow burst event observed by Cluster, *Geophys. Res. Lett.*, 29(20), 1942, doi:10.1029/2002GL015763, 2002.
- [28] Nagai, T., I. Shinohara, M. Fujimoto, S. Machida, R. Nakamura, Y. Saito, and T. Mukai, Structure of the Hall current system in the vicinity of the magnetic reconnection site, *J. Geophys. Res.*, 108(A10), doi:10.1029/2003JA009900, 2003.

- [29] Neagu, E., J. E. Borovsky, M. F. Thomsen, S. P. Gary, W. Baumjohann, and R. A. Treumann, Statistical survey of magnetic field and ion velocity fluctuations in the near-Earth plasma sheet: Active Magnetospheric Particle Trace Explorers/Ion Release Module (AMPTE/IRM) measurements, *J. Geophys. Res.*, *107*(A7), doi:10.1029/2001JA000318, 2002.
- [30] Ohtani, S., T. Higuchi, A. T. Y. Lui, and K. Takahashi, Magnetic fluctuations associated with tail current disruption: Fractal analysis, *J. Geophys. Res.*, *100*, 19135, 1995.
- [31] Oughton, S., E. R. Priest and W. H. Matthaeus, The influence of a mean magnetic field on three-dimensional magnetohydrodynamic turbulence, *J. Fluid Mech.*, *280*, 95, 1994.
- [32] Réme, H., et al., First multispacecraft ion measurements in and near the Earth's magnetosphere with the identical Cluster ion spectrometry (CIS) experiment, *Ann. Geophys.*, *19*, 1303, 2001.
- [33] Runov, A., et al., Current sheet structure near magnetic X-line observed by Cluster, *Geophys. Res. Lett.*, *30*(11), 1579, doi:10.1029/2002GL016730, 2003.
- [34] Schödel, R., W. Baumjohann, R. Nakamura, V. A. Sergeev, and T. Mukai, Rapid flux transport in the central plasma sheet, *J. Geophys. Res.*, *106*, 301, 2001.
- [35] Sergeev, V. A., V. Angelopoulos, J. T. Gosling, C. A. Cattell, and C. T. Russell, Detection of localized, plasma-depleted flux tubes or bubbles in the midtail plasma sheet, *J. Geophys. Res.*, *101*, 10817, 1996.
- [36] Shebalin, J. V., W. H. Matthaeus, and D. C. Montgomery, Anisotropy in MHD turbulence due to a mean magnetic field, *J. Plasma Phys.*, *29*, 525, 1983.
- [37] Veitch, D., and P. Abry, A wavelet based joint estimator of the parameters of long-range dependence, *IEEE Trans. Inf. Theor.*, *45*, 878, 1999.
- [38] Volwerk, M., et al., A statistical study of compressional waves in the tail current sheet, *Geophys. Res. Lett.*, *108*(A12), 1429, doi:10.1029/2003JA010155, 2003.
- [39] Volwerk, M., et al., Compressional waves in the neutral sheet, *Ann. Geophys.*, *22*, 303, 2004.
- [40] Vörös, Z., et al., Multi-scale magnetic field intermittence in the plasma sheet, *Ann. Geophys.*, *21*, 1955, 2003.

- [41] Vörös, Z., et al., Wavelet analysis of magnetic turbulence in the Earth's plasma sheet, *Phys. Plasmas*, *11*, 1333, doi: 10.1063/1.1667499, 2004.
- [42] Watkins, N. W., M. P. Freeman, C. S. Rhodes, and G. Rowlands, Ambiguities in determination of self-affinity in the AE-index time series, *Fractals*, *9*, 471, 2001.



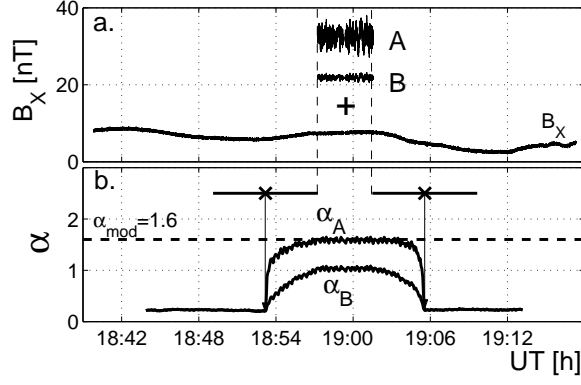


Figure 1: Estimation of the scaling index  $\alpha$ ; (a) Fractal signals A and B to be embedded and quiet time  $B_X$  measured by Cluster 3 on September 7, 2001; the generated fractal signals A and B have the same  $\alpha_{mod} = 1.6$ , but different amplitudes, (b)  $\alpha_A$  and  $\alpha_B$  from mixed signal; (the dashed line corresponds to the theoretical value  $\alpha_{mod} = 1.6$ )

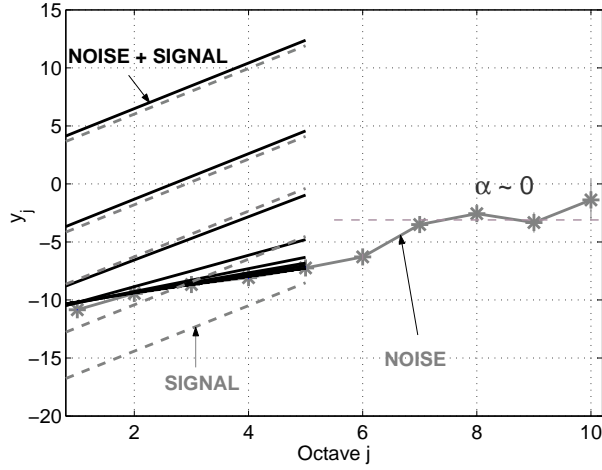


Figure 2: The logscale diagram; The scaling properties of signal, noise and signal+noise cases are shown when the signal to noise ratio is changed;  $y_j \equiv \log_2 \mu_j$  (Eq.1)

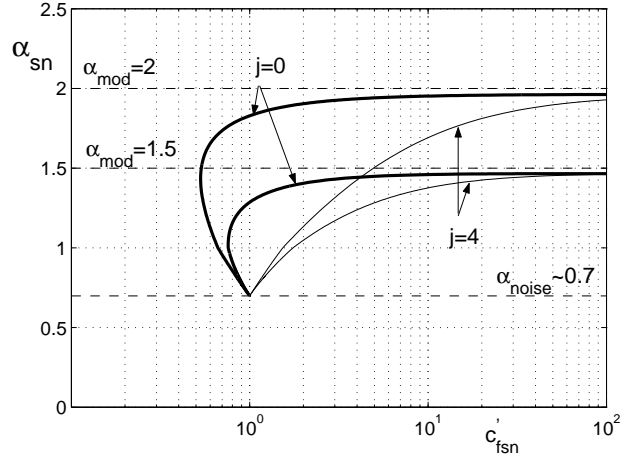


Figure 3: The  $\alpha_{sn}(c'_{fsn})$  relationship (correction curves) for model fractal signals with  $\alpha_{mod} = 1.5$  and  $2$ , computed at the octaves  $j = 0$  and  $j = 4$

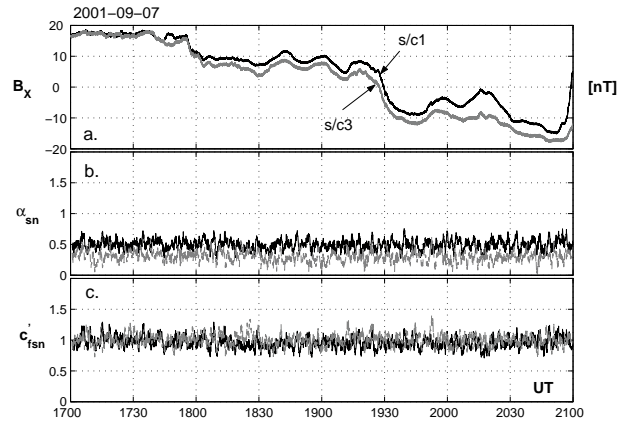


Figure 4: Estimation of the quiet time noise level of the scaling parameters; a.)  $B_X$  component of the magnetic field on September 7, 2001 b.)  $\alpha_{sn}$  c.)  $c'_{fsn}$ ; all for s/c 1 and 3

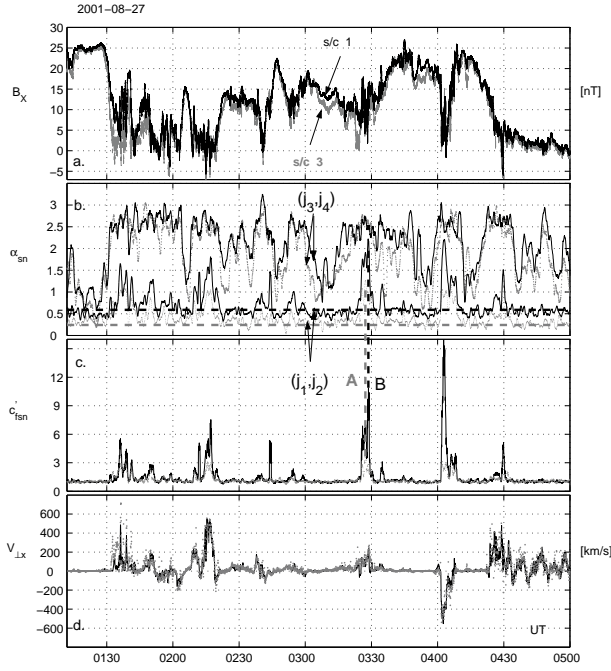


Figure 5: Two-point (s/c 1,3) estimation of the scaling parameters in comparison with the magnetic field and velocity measurements; a.) the  $B_X$  components of the magnetic field; b.)  $\alpha_{sn}$  estimated at small scales  $(j_1, j_2) \sim (0.08, 0.33)s$  and at large scales  $(j_3, j_4) = (0.7, 5)s$ ; c.)  $(c'_{f sn})$  estimated at the scale  $j = 4 \sim 0.33 s$ ; the capital letters A and B show two cases when corrections to small-scale  $\alpha$  are introduced in Figure 6; d.) x-component of perpendicular velocity

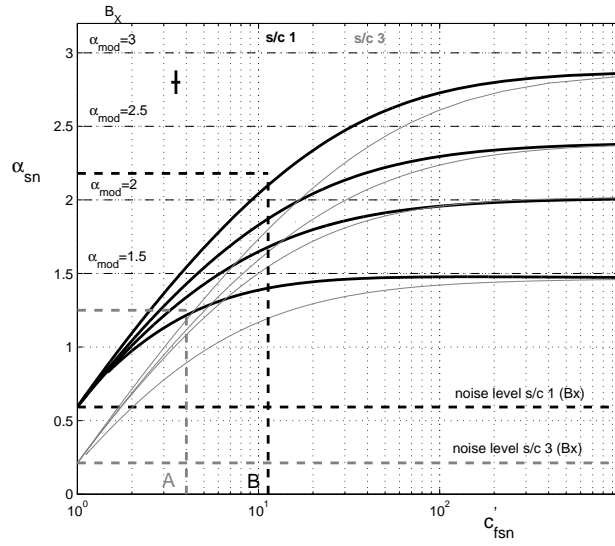


Figure 6: Correction curves computed for model fractals with  $\alpha_{mod} = 1.5, 2, 2.5, 3$ ; the correction curves reach asymptotically the theoretical values  $\alpha_{mod}$  for  $c'_{fsn} \rightarrow \infty$  and the noise level for  $c'_{fsn} \rightarrow 1$ ; the letter A corresponds to s/c 3 while B to s/c 1; the error bars at the left-top corner arise from the uncertainty of parameter estimation in logscale diagram and from the uncertainty of the magnetometer noise level estimation

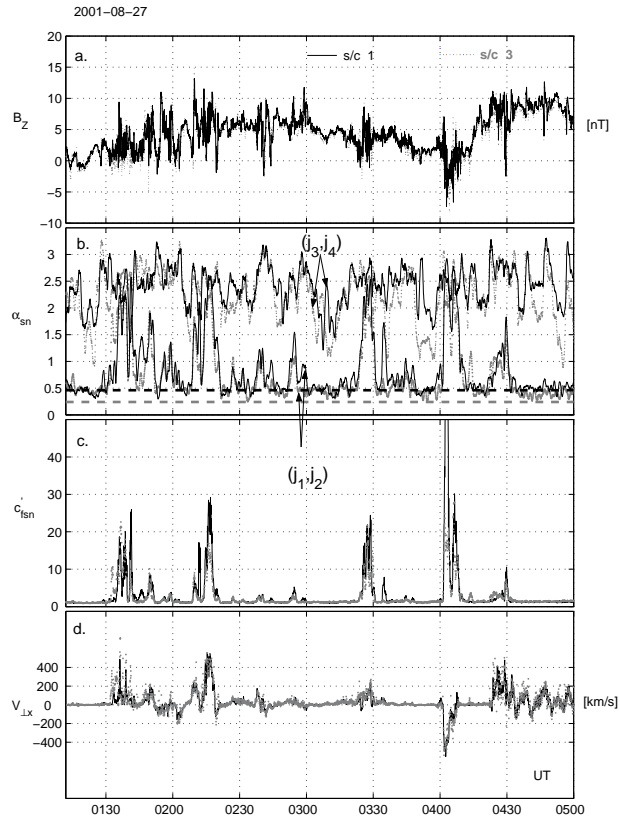


Figure 7: Same as in Figure 5, but for the  $B_Z$  component of magnetic field

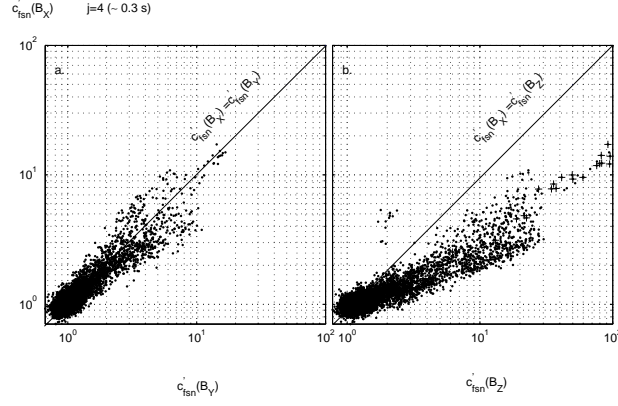


Figure 8: Log-log scatterplots of powers at the scale  $j = 4 \sim 0.33$  s; a.)  $c'_{fsn}(B_X)$  versus  $c'_{fsn}(B_Y)$ ; b.)  $c'_{fsn}(B_X)$  versus  $c'_{fsn}(B_Z)$  - the crosses correspond to an interval of magnetic reconnection

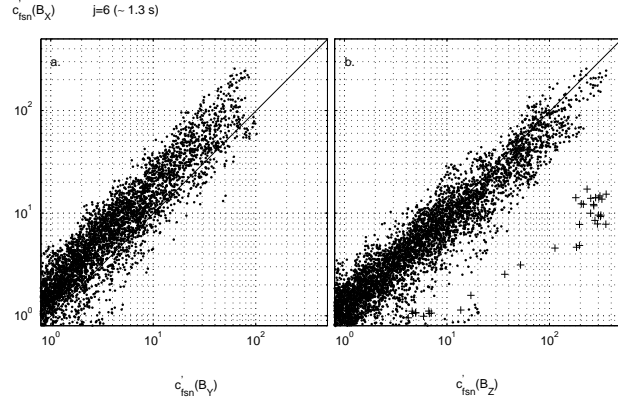


Figure 9: Log-log scatterplots of powers at the scale  $j = 6 \sim 1.3$  s; a.)  $c'_{fsn}(B_X)$  versus  $c'_{fsn}(B_Y)$ ; b.)  $c'_{fsn}(B_X)$  versus  $c'_{fsn}(B_Z)$  - the crosses correspond to an interval of magnetic reconnection

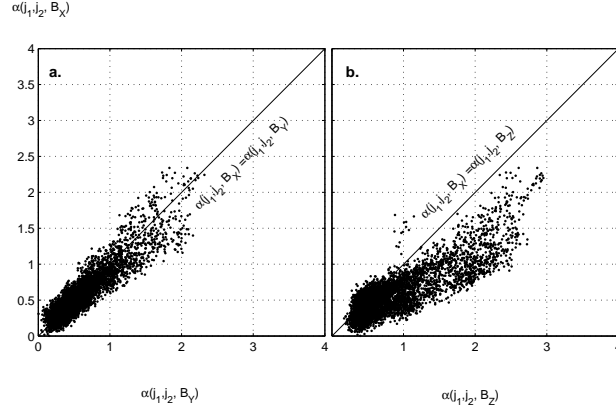


Figure 10: Small-scale  $(j_1, j_2)$  scatterplots of the scaling indices; a.)  $\alpha_{sn}(B_X)$  versus  $\alpha_{sn}(B_Y)$ ; b.)  $\alpha_{sn}(B_X)$  versus  $\alpha_{sn}(B_Z)$

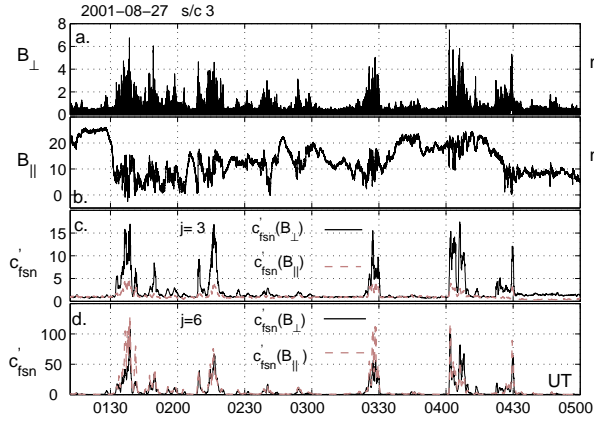


Figure 11: Magnetic fluctuations in the mean magnetic field coordinate system; a.) the perpendicular component ( $B_{\perp}$ ); b.) the parallel component ( $B_{\parallel}$ ); c.) the normalized powers of  $B_{\perp}$  and  $B_{\parallel}$  at the time scale 0.33s; d.) the normalized powers of  $B_{\perp}$  and  $B_{\parallel}$  at the time scale 1.3s;

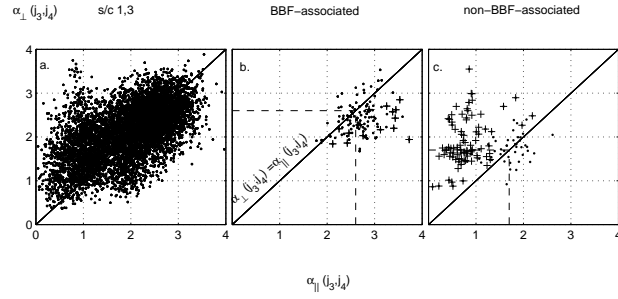


Figure 12: Joint conditional statistics in a coordinate system parallel and perpendicular to the local mean magnetic field at scales  $(j_3, j_4)$ ; a.) scatterplot of all available points from s/c 1,3; b.) scatterplot of BBF-associated data points - the crosses correspond to an interval of magnetic reconnection; c.) scatterplot of non-BBF-associated data points - the crosses correspond to the intervals when  $|B_X| > 20$  nT, while the points represents intervals with  $|B_X| \leq 15$  nT